Engineering Analysis with Boundary Elements 163 (2024) 474–481

Contents lists available at ScienceDirect

Engineering Analysis with Boundary Elements

journal homepage: www.elsevier.com/locate/enganabound

A stable Generalized Finite Element Method for stokes interface problems

Haodi Zhu [a], Jianping Zhao [a,b,*], Yanren Hou [a,c]

[a] College of Mathematics and System Sciences, Xinjiang University, Urumqi 830046, China
[b] Institute of Mathematics and Physics, Xinjiang University, Urumqi 830046, China
[c] School of Mathematics and Statistics, Xi'an Jiaotong University, Xi'an 710049, China

ARTICLE INFO

Keywords:
GFEM
SGFEM
Stokes equations
Interface problems
Condition number

ABSTRACT

The Generalized Finite Element Method (GFEM) is developed from the Partition of the Unity Method (PUM), which expands the standard finite element space by using non-polynomial function spaces called the enrichment spaces. GFEM has been successfully applied to various problems, but it still has some drawbacks. It lacks robustness in adjusting meshes when solving interface problems, and the condition number of the stiffness matrix will increase dramatically when the interface is close to the mesh boundary. This phenomenon can lead to ill-conditioned linear equations. A stable GFEM called SGFEM is proposed for the Stokes interface problem in this paper, which modifies the enrichment space. The SGFEM space of the velocity is divided into a basic part $\mathbb{S}_{FEM}$ and an enrichment part $\mathbb{S}^*_{ENR}$. The discretization of space $(\mathbb{S}_{FEM} \times \mathbb{Q}_h)$ uses $Q_1 - Q_0$ element or the Taylor-Hood element for the study. $\mathbb{S}^*_{ENR}$ uses different interpolation functions. Numerical studies show that SGFEM has the optimal convergence order of the error and robustness. The growth rate of the scaled condition number of the stiffness matrix is the same as that of a standard FEM.

1. Introduction

Partial differential equation models appear in many real world applications, such as elastodynamics, fluid mechanics, materials science, etc. Among them problems with discontinuous coefficients and interfaces are important research topics. Discontinuous problems include crack extensions, fluid–structure couplings, multiphase flows and flows in porous media, etc. For two-phase flow problems, the Navier–Stokes equation with discontinuous viscosity coefficients (interface problem) is a frequently encountered model. If the viscosities of a two-phase flow are large, the Stokes equation with discontinuous viscosity coefficients is a more convenient model. In this paper, we adopt the Stable Generalized Finite Element Method (SGFEM) to solve the Stokes interface problem.

Let $\Omega \subset \mathbb{R}^2$ be a bounded, simply connected domain with a smooth boundary $\partial\Omega$. Consider two subdomains, denoted as $\Omega_1 \subset \Omega$ and $\Omega_2 \subset \Omega$, which satisfy $\Omega_1 \cap \Omega_2 = \emptyset$, $\overline{\Omega}_1 \cup \overline{\Omega}_2 = \Omega$. The interface is defined as the boundary between the two subdomains, denoted as $\overline{\Omega}_1 \cap \overline{\Omega}_2 = \Gamma$. This paper discusses circular interface and straight interface problems, as shown in Fig. 1. Consider the Stokes interface problems

$$\begin{aligned} -\nabla \cdot (2\mu\epsilon(\mathbf{u})) + \nabla p &= \mathbf{f}, \quad \text{in } \Omega_1 \cup \Omega_2, \\ \nabla \cdot \mathbf{u} &= 0, \quad \text{in } \Omega, \end{aligned} \tag{1.1}$$

with the Dirichlet boundary condition

$$\mathbf{u} = \mathbf{g}_D, \quad \text{on } \partial\Omega, \tag{1.2}$$

where $\mathbf{u}$ is the velocity, p is the pressure, $\mathbf{f}$ is the body force and $\epsilon(\mathbf{u}) = \frac{1}{2}(\nabla\mathbf{u} + (\nabla\mathbf{u})^T)$ is the strain tensor. Assume that the viscosity coefficient $\mu(\mathbf{x})$ is a piecewise constant,

$$\mu = \begin{cases} \mu_1, & \text{in } \Omega_1, \\ \mu_2, & \text{in } \Omega_2, \end{cases}$$

and the jump conditions are

$$\begin{aligned} [\mathbf{u}]_\Gamma &= 0, \quad \text{on } \Gamma, \\ [\boldsymbol{\sigma}(\mu, \mathbf{u}, p)\mathbf{n}]_\Gamma &= 0, \quad \text{on } \Gamma, \end{aligned} \tag{1.3}$$

where the $\boldsymbol{\sigma}(\mu, \mathbf{u}, p) = 2\mu\epsilon(\mathbf{u}) - p\mathbb{I}$ is the stress tensor, $\mathbb{I}$ is the identity matrix, $\mathbf{n}$ is the unit normal vector to the interface Γ pointing to the region outside the circle or on a straight line, and $[\mathbf{v}]_\Gamma$ denotes the jump of the function $\mathbf{v}(x)$ across the interface, i.e.$[\mathbf{v}(\mathbf{x})] = \mathbf{v}_{\mathbf{1}(\mathbf{x})}|_\Gamma - \mathbf{v}_{\mathbf{2}(\mathbf{x})}|_\Gamma$. Here $\mathbf{v}_{\mathbf{1}(\mathbf{x})} = \mathbf{v}(\mathbf{x})|_{\Omega_1}$ and $\mathbf{v}_{\mathbf{2}(\mathbf{x})} = \mathbf{v}(\mathbf{x})|_{\Omega_2}$. In addition, the second equation in (1.1) provides an additional condition for jumps across the interface

$$[\nabla \cdot \mathbf{u}]|_\Gamma = 0, \quad \text{on } \Gamma.$$

The non body-fitted mesh methods for interface problems include Immersed Interface Method (IIM), Immersed Finite Element Method (IFEM), Generalized Finite Element Method (GFEM), or Extended Finite Element Method (XFEM), etc. In 1972, Peskin proposed the Immersed

* Corresponding author at: College of Mathematics and System Sciences, Xinjiang University, Urumqi 830046, China.
E-mail address: jpzhao@xju.edu.cn (J. Zhao).

https://doi.org/10.1016/j.enganabound.2024.03.025
Received 8 December 2023; Received in revised form 19 March 2024; Accepted 19 March 2024
Available online 4 April 2024

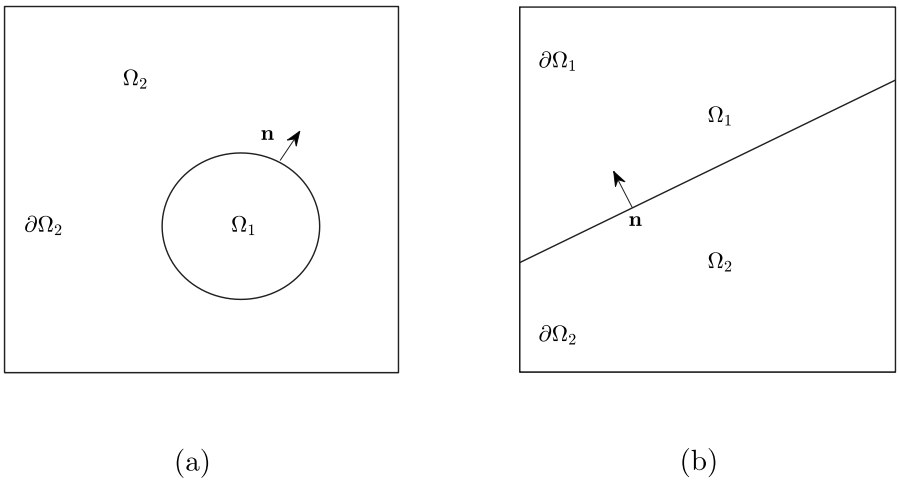

Fig. 1. Diagram of different interfaces: (a) A circular interface. (b) A straight line interface.

Boundary Method (IBM) to solve the blood flow in the heart [1]. The main idea is to use a uniform mesh and use a continuous function to smoothly connect the solutions to be solved on both sides of the interface, resulting in a numerical method with first-order accuracy. This breakthrough enabled significant progress in numerical simulations of interface problems. In 1994, Li and LeVeque proposed the IIM [2], which constructs a second-order numerical method for solving elliptic interface problems based on finite differences. The authors in [3] improved IIM by using piecewise quadratic polynomials. In the field of finite element methods, the earliest work for elliptic equations with discontinuous coefficients was presented by Babuška [4], with the aim of dealing with the problem of discontinuous coefficients.

In 1996, Melenk and Babuška proposed the Partition of the Unity Method (PUM) [5]. It is a groundbreaking work. In the following decades, the GFEM and XFEM have been developed based on PUM with the aim of constructing numerical methods for solving discontinuous problems and have been widely used to solve various types of problems. Among them, XFEM was first proposed in 1999 by J. E. Dolbow [6] and Ted Belytschko and Blacks [7], with the idea of using independent meshes for solving crack extensions and adding expanding shape functions near the crack surfaces or tips. Quasi-static cracks, multi-cracks, and hole models were studied in [8,9]. PUM was called GFEM in [10–12] and GFEM is the PUM with a special PU. It was later recognized that the two methods are equivalent and the condition number of the stiffness matrix in GFEM/XFEM can be large, leading to ill-conditioned systems in [13]. And GFEM may be unstable and lacks robustness in adjusting meshes. In [14], Hansbo first proposed a new method for elliptic interface problems called Nitsche-XFEM, which combines the Nitsche method with the extended finite element method and achieves uniform optimal convergence order with respect to the interface location. They later applied this method to Stokes interface problems, as seen in [15,16]. More studies on the interface problems of the Stokes equation can be found in [17–20].

In 2012, Babuška proposed the Stable Generalized Finite Element Method (SGFEM) [21], which solves the ill-conditioned system issue in GFEM. He starts from the construction of the finite element space and argues that if the enrichment function space is orthogonal or almost orthogonal to the standard function space, the condition number of the stiffness matrix and the convergence order of the error are the same as those of the standard FEM. The main idea is to modify the enrichment space by subtracting the interpolation of the enrichment function. In [22], a definition was proposed: if the "angle" between the enrichment space and the standard space is significantly larger than 0 with respect to the mesh, GFEM is called SGFEM. In 2013, the stabilization idea was applied to the pressure-discontinuous Navier–Stokes interface problem [23], and the enrichment function used a symbol distance function, namely

$$\psi(\mathbf{x},t)=\operatorname{sign}(\phi(\mathbf{x},t))=\begin{cases}-1, & \phi(\mathbf{x},t)<0,\\ 0, & \phi(\mathbf{x},t)=0,\\ 1, & \phi(\mathbf{x},t)>0,\end{cases}$$

where $\phi(\mathbf{x},t)$ is the level set function of the interface. In [24], the authors applied SGFEM to 3D fracture mechanics. The two degree SGFEM for interface problems and higher-order SGFEM are investigated by Zhang and Babuška et al. [25,26]. And they applied it to elliptic interface problems and parabolic interface problems, respectively [22,27,28]. Among them, the authors in [28] modified the enrichment function $D(\mathbf{x})=dist(\mathbf{x},\Gamma)$ to a one-sided distance function, namely

$$\tilde{D}(\mathbf{x}):=\begin{cases}D(\mathbf{x}), & \mathbf{x}\in\Omega_1,\\ 0, & \mathbf{x}\in\Omega_2.\end{cases}$$

where Ω_1 and Ω_2 are two areas separated by the interface. In order to further investigate the stability and robustness of SGFEM, as well as explore different interpolation functions in the stabilization approach, this paper extends SGFEM to the interface problem of the Stokes equation.

The organization of this paper is as follows. In Section 2, we present some notations and make a brief introduction to GFEM. The detailed algorithm for solving the Stokes interface problem by SGFEM is described in Section 3. And the weak form is modified by adding a penalty for the study of the scaled condition number. In Section 4, The convergence and robustness of SGFEM are analyzed through numerical examples. Finally, Section 5 provides the conclusion of this paper.

2. Preliminaries

Discontinuities are usually categorized into strong and weak discontinuities, which refer to the discontinuity of the solution and the discontinuity of its gradient across the interface, respectively. From the interface condition (1.3), $\mathbf{u}$ is continuous on the interface Γ, while its gradient is discontinuous on the interface due to the discontinuous viscosity coefficient μ. And we assume that the pressure p is continuous. In this paper, more attention is paid to the weak discontinuity of the velocity $\mathbf{u}$. In fact, the pressure p may also involve jumps across the interface.

2.1. Notations

Denote the standard Sobolev spaces by $W_m^k(\Omega)$ with the norm $\|\cdot\|_{W_m^k(\Omega)}$ and the seminorm $|\cdot|_{W_m^k(\Omega)}$. As usual, using $H^k(\Omega)$, $\|\cdot$

$\|\cdot\|_{H^k(\Omega)}$, $|\cdot|_{H^k(\Omega)}$ to describe the above items respectively for $m = 2$ and $L^2(\Omega)$, $\|\cdot\|_{L^2(\Omega)}$, $|\cdot|_{L^2(\Omega)}$ for $k = 0, m = 2$. Specially, $H_0^1(\Omega) = \{\mathbf{v} \in H^1(\Omega) : \mathbf{v} = 0 \text{ on } \partial\Omega\}$. Next we define the velocity space and the pressure space as follows:

$$\mathbb{V} = \left[H_0^1(\Omega)\right]^2, \quad \mathbb{Q} = \left\{q \in L^2(\Omega) : \int_\Omega q \, d\Omega = 0\right\}.$$

Then the weak formulation of the problem (1.1)–(1.2) is to find $(\mathbf{u}, p) \in \mathbb{V} \times \mathbb{Q}$ such that

$$\begin{aligned} \mathcal{A}(\mathbf{u}, \mathbf{v}) \; + \; \mathcal{B}(\mathbf{v}, p) \; &= \; (\mathbf{f}, \mathbf{v}), \\ \mathcal{B}(\mathbf{u}, q) \; &= \; 0, \end{aligned} \tag{2.1}$$

for any $(\mathbf{v}, q) \in \mathbb{V} \times \mathbb{Q}$, where

$$\begin{aligned} \mathcal{A}(\mathbf{u}, \mathbf{v}) &= \int_\Omega 2\mu\epsilon(\mathbf{u}) : \epsilon(\mathbf{v}) \, d\Omega \; , \quad \mathcal{B}(\mathbf{v}, p) \\ &= -\int_\Omega q\nabla \cdot \mathbf{v} \, d\Omega \; , \quad (\mathbf{f}, \mathbf{v}) = \int_\Omega \mathbf{f} \cdot \mathbf{v} \, d\Omega, \end{aligned}$$

with

$$\begin{aligned} A : B &= \begin{pmatrix} a_{11} & a_{12} \\ a_{21} & a_{22} \end{pmatrix} : \begin{pmatrix} b_{11} & b_{12} \\ b_{21} & b_{22} \end{pmatrix} \\ &= a_{11}b_{11} + a_{12}b_{12} + a_{21}b_{21} + a_{22}b_{22}. \end{aligned}$$

In addition, we define the energy norm $\|\cdot\|_{\mathscr{E}(\Omega)}$ by

$$\|\mathbf{v}\|_{\mathscr{E}(\Omega)}^2 = \int_\Omega \mu\nabla\mathbf{v} \cdot \nabla\mathbf{v} \, d\Omega.$$

Remark 1. When using the finite element method to solve the Stokes equation without interface, if the linear element is used for velocity $\mathbf{u}$ and the piecewise constant for pressure p, the convergence orders of the L^2 error for $\mathbf{u}$, the energy error for $\mathbf{u}$ and the L^2 error for p are $O(h^2)$, $O(h)$ and $O(h)$, respectively. If $\mathbf{u}$ is the quadratic element and p is the linear element, they are $O(h^3)$, $O(h^2)$ and $O(h^2)$, respectively [29].

2.2. GFEM

GFEM is the PUM with a special PU. Compared to the traditional FEM, GFEM does not require meshes redivision or refinement. The meshes are independent and fixed.

Let $\mathcal{T}_h$ be the uniform mesh on Ω with nodes $\mathbf{x}_i$, $i \in I_h$, where I_h is the index set of the nodes and $\mathbf{x}_i = (x_i, y_i)^T$. The elements τ_s related to the mesh $\mathcal{T}_h$ are closed quadrilaterals and their set is described as $\{\tau_s : s \in E_h\}$, where E_h is the index of the elements. For an element τ_s, $\{\mathbf{x}_i : i \in I_h^s\}$ are all nodes of it, where $I_h^s \subset I_h$ is the index set. Similarly we define the set of all elements associated with the node $\mathbf{x}_i$ as $\{\tau_s : s \in E_h^i \in E_h\}$. In addition, we use E_Γ to denote the index set of the elements intersecting the interface, namely $E_\Gamma = \{s : \tau_s \cap \Gamma \neq \emptyset\}$.

We enrich the space of velocity $\mathbf{u}$ if the GFEM is used for the spatial approximation of the variational (2.1).

2.2.1. Q_1 and Q_0

The standard FEM space uses Q_1 element and Q_0 element, namely the velocity $\mathbf{u}$ uses the Q_1 element and the pressure p uses Q_0 element. Then, the velocity and the pressure approximation spaces are defined as follow:

$$\begin{aligned} &\mathbb{S}_{FEM}^1 = \mathbb{V}_h^1 = \text{span}\{N_i^u : N_i^u \text{ is the bilinear Lagrange basis function}, i \in I_h^u\}, \\ &\mathbb{S}_{ENR}^1 = \text{span}\{wN_i^u : N_i^u \text{ is bilinear}, \; i \in I_{ENR} \subset I_h^u\}, \\ &\mathbb{S}_{GFEM}^1 = \mathbb{S}_{FEM}^1 \oplus \mathbb{S}_{ENR}^1 = \{\mathbf{v} = \mathbf{v}_1 + \mathbf{v}_2 : \mathbf{v}_1 \in \mathbb{S}_{FEM}^1, \mathbf{v}_2 \in \mathbb{S}_{ENR}^1\}, \end{aligned}$$

and

$$\mathbb{Q}_h^0 = \text{span}\{1\}.$$

2.2.2. Taylor-Hood

The standard FEM space uses Taylor-Hood element, namely the velocity $\mathbf{u}$ uses the Q_2 element and the pressure p uses Q_1 element. Then the velocity and the pressure approximation spaces are defined as follows:

$$\begin{aligned} &\mathbb{S}_{FEM}^2 = \mathbb{V}_h^2 = \text{span}\{N_i^u : N_i^u \text{ is the biquadratic Lagrange basis function}, i \in I_h^u\}, \\ &\mathbb{S}_{ENR}^2 = \text{span}\{wN_i^u : N_i^u \text{ is biquadratic}, \; i \in I_{ENR} \subset I_h^u\}, \\ &\mathbb{S}_{GFEM}^2 = \mathbb{S}_{FEM}^2 \oplus \mathbb{S}_{ENR}^2 = \{\mathbf{v} = \mathbf{v}_1 + \mathbf{v}_2 : \mathbf{v}_1 \in \mathbb{S}_{FEM}^2, \mathbf{v}_2 \in \mathbb{S}_{ENR}^2\}, \end{aligned}$$

and

$$\mathbb{Q}_h^1 = \text{span}\{N_i^p : N_i^p \text{ is the bilinear Lagrange basis function}, i \in I_h^p\}.$$

Since the pressure p is continuous, only the velocity space is enriched. We call $\mathbb{S}_{ENR}^k$ the enrichment space of GFEM, $w(\mathbf{x})$ the enrichment function, and $\{\mathbf{x}_i, i \in I_{ENR}\}$ the enrichment nodes. I_h^u and I_h^p are the index sets of the finite element nodes of the discretized $\mathbf{u}$ and p, respectively. They are related to the form of the basis functions. Note that I_h^u does not include enrichment nodes. We use N_i^u and N_i^p to represent the shape functions for $\mathbf{u}$ and p uniformly in the following. For the convenience of discussions, $\mathbb{S}_{GFEM}$ is uniformly represented as

$$\mathbb{S}_{GFEM}^k = \mathbb{S}_{FEM}^k \oplus \mathbb{S}_{ENR}^k = \{\mathbf{v} = \mathbf{v}_1 + \mathbf{v}_2 : \mathbf{v}_1 \in \mathbb{S}_{FEM}^k, \mathbf{v}_2 \in \mathbb{S}_{ENR}^k\}, \quad k = 1, 2. \tag{2.2}$$

Different GFEM can be obtained by selecting different enrichment functions and enrichment nodes. For the problems of weak discontinuities, the enrichment function is chosen to be

$$w(\mathbf{x}) = dist(\mathbf{x}, \Gamma).$$

Clearly, $w(\mathbf{x})$ is continuous on Ω and $w(\mathbf{x}) = 0$ for $\mathbf{x} \in \Gamma$. If we do not enrich the space of the FEM, the space of the GFEM is a standard finite element space, namely

$$\mathbb{S}_{GFEM}^k = \mathbb{S}_{FEM}^k = \mathbb{V}_h^k, \quad k = 1, 2.$$

3. The stable GFEM and the scaled condition number

In the previous application of the GFEM to interface problems (1.1), it tends to produce ill-conditioned stiffness matrix. Especially when the interface is very close to the mesh, the condition number of the stiffness matrix will increase sharply. As shown in Fig. 2, S_{cut} represents the smaller area formed when the support of the enrichment node $\mathbf{x}_i$ is cut by the interface. $S_{support}$ represents the area of the support of $\mathbf{x}_i$, namely the sum of the areas of the four rectangles. If

$$S_{cut} < CS_{support} \text{ and } C \ll 1,$$

the usual approach is to no longer expand this node, which avoids the rapid increase of the stiffness matrix condition number. But the numerical process is relatively cumbersome. The SGFEM avoids this problem in the numerical process.

3.1. The SGFEM for Stokes interface problem

In 2012, Babuška proposed the SGFEM [21]. The idea is to subtract the interpolation of the enrichment function $w(\mathbf{x})$ from itself, namely

$$w^*(\mathbf{x}) = w(\mathbf{x}) - \mathcal{I}_h w(\mathbf{x}),$$

where $\mathcal{I}_h w(\mathbf{x})$ is a piecewise linear or quadratic interpolation of $w(\mathbf{x})$. Particular attention should be paid to the choice of the interpolation function $\mathcal{I}_h w(\mathbf{x})$ in $w^*(\mathbf{x})$. The two degree SGFEM for the interface problems was investigated in [25]. The form restricted to the element τ_s is

$$\mathcal{I}_{\tau_s} w(\mathbf{x}) = \sum_{k=1}^{n_u} w(\mathbf{x}_k) N_k^u \Big|_{\tau_s}, \quad s \in E_\Gamma,$$

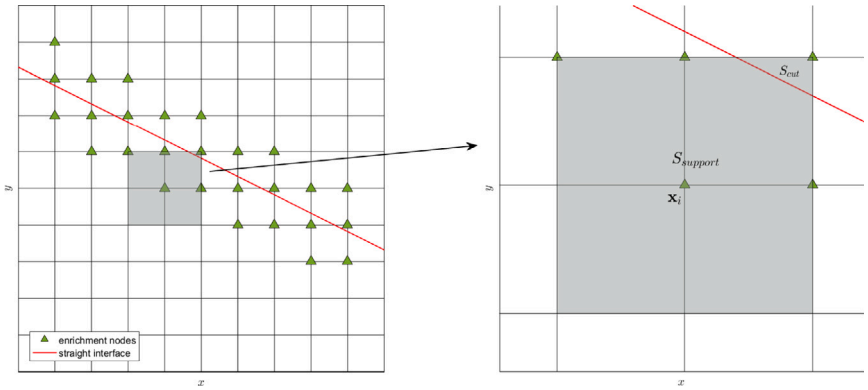

Fig. 2. Enrichment strategy for GFEM.

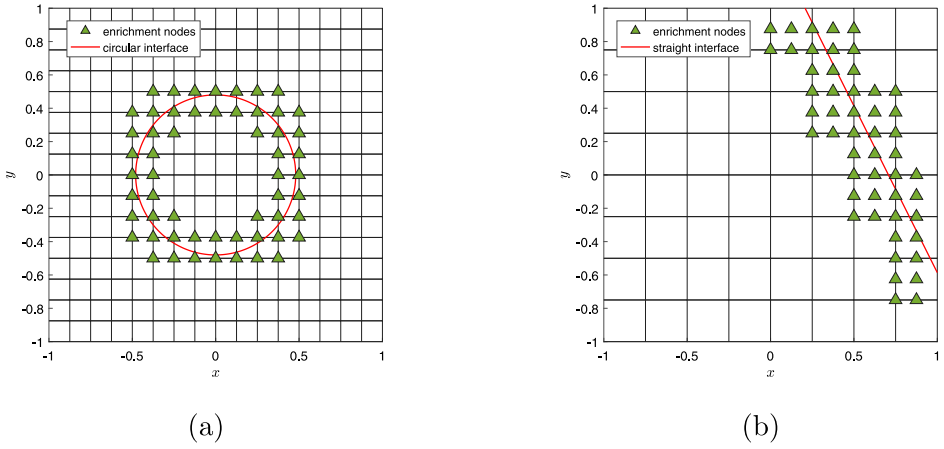

Fig. 3. An illustration of the enrichment nodes $\{\mathbf{x}_i : i \in I_\Gamma\}$: (a) Circular and bilinear discretization. (b) Straight and biquadratic discretization.

where n_u is the number of the finite element nodes in τ_s, which is related to N_k^u being a linear or quadratic function. Clearly, the support of $w^*(\mathbf{x})$ is

$$supp\{w^*(\mathbf{x})\} = \bigcup_{s\in E_\Gamma} \tau_s.$$

Remark 2. Let I_Γ represent the index set of the finite element nodes of the element $\{\tau_s : s \in E_\Gamma\}$. Note that for the condition (1.2) of the straight interface problem, I_Γ does not include the nodes on $\partial\Omega$. The selection of enrichment nodes is given by $I_{ENR} = I_\Gamma$ in SGFEM, as shown in Fig. 3. The green triangles in the graph represent an enrichment nodes.

After modifying the enrichment function and determining the enrichment nodes, we define the SGFEM space of velocity as

$$\mathbb{S}^k_{SGFEM} = \mathbb{S}^k_{FEM} \oplus \mathbb{S}^{k*}_{ENR} \quad \text{and} \quad \mathbb{S}^{k*}_{ENR} = \text{span}\{w^* N_i^u,\ i \in I_\Gamma\},\ \ k = 1, 2.$$

The N_i^u in $\mathbb{S}^{k*}_{ENR}$ and the N_k^u in I_h are bilinear for $k = 1$ and biquadratic for $k = 2$. In the case of continuous pressure, the discretized spaces for velocity and pressure are denoted as $\mathbb{S}^k_{SGFEM}$ and $\mathbb{Q}_h^{k-1}$, $k = 1, 2$, respectively.

The same Lagrange basis functions N_i^u are used as the PU in $\mathbb{S}^k_{FEM}$ and $\mathbb{S}^{k*}_{ENR}$, and we choose the interpolation function of the same order as it. After adding additional degrees of freedom, the forms of the velocity solution $\mathbf{u}_h$ and the pressure solution p_h are given by

$$\mathbf{u}_h = \sum_{i\in I_h^u} \boldsymbol{a}_i N_i^u + \sum_{k\in I_\Gamma} \boldsymbol{b}_k w^* N_k^u,$$

$$p_h = \sum_{i\in I_h^p} p_i N_i^p,$$

where $\mathbf{u}_h = (u_{1h}, u_{2h})^T$, $\boldsymbol{a}_i = (a_{1i}, a_{2i})^T$, $\boldsymbol{b}_k = (b_{1k}, b_{2k})^T$. This leads to solving the following linear system

$$AU = F,$$

where

$$A = \begin{bmatrix} A_{11} & A_{12} & A_{13} & A_{14} & A_{15} \\ A_{12}^T & A_{22} & A_{23} & A_{24} & A_{25} \\ A_{13}^T & A_{23}^T & A_{33} & A_{34} & A_{35} \\ A_{14}^T & A_{24}^T & A_{34}^T & A_{11}^{enr} & A_{12}^{enr} \\ A_{15}^T & A_{25}^T & A_{35}^T & A_{21}^{enr} & A_{22}^{enr} \end{bmatrix}, \quad U = \begin{bmatrix} \overrightarrow{a_1} \\ \overrightarrow{a_2} \\ \overrightarrow{p} \\ \overrightarrow{b_1} \\ \overrightarrow{b_2} \end{bmatrix}, \quad F = \begin{bmatrix} F_1 \\ F_2 \\ 0 \\ F_1^{enr} \\ F_2^{enr} \end{bmatrix}.$$

Details as follows:

$$\begin{bmatrix} A_{11} & A_{12} \\ A_{12}^T & A_{22} \end{bmatrix} = \begin{bmatrix} \mathcal{A}\left(\begin{pmatrix} N_j^u \\ 0 \end{pmatrix}, \begin{pmatrix} N_i^u \\ 0 \end{pmatrix}\right) & \mathcal{A}\left(\begin{pmatrix} 0 \\ N_j^u \end{pmatrix}, \begin{pmatrix} N_i^u \\ 0 \end{pmatrix}\right) \\ \mathcal{A}\left(\begin{pmatrix} N_j^u \\ 0 \end{pmatrix}, \begin{pmatrix} 0 \\ N_i^u \end{pmatrix}\right) & \mathcal{A}\left(\begin{pmatrix} 0 \\ N_j^u \end{pmatrix}, \begin{pmatrix} 0 \\ N_i^u \end{pmatrix}\right) \end{bmatrix}_{i,j\in I_h^u},$$

$$\begin{bmatrix} A_{13} \\ A_{23} \end{bmatrix} = \left[\mathcal{B}\left(\begin{pmatrix} N_i^u \\ 0 \end{pmatrix}, N_j^p\right)\ \mathcal{B}\left(\begin{pmatrix} 0 \\ N_i^u \end{pmatrix}, N_j^p\right)\right]^T_{i\in I_h^u, j\in I_h^p},$$

$$\begin{bmatrix} A_{14} & A_{15} \\ A_{24} & A_{25} \end{bmatrix} = \begin{bmatrix} \mathcal{A}\left(\begin{pmatrix} w^* N_k^u \\ 0 \end{pmatrix}, \begin{pmatrix} N_i^u \\ 0 \end{pmatrix}\right) & \mathcal{A}\left(\begin{pmatrix} 0 \\ w^* N_k^u \end{pmatrix}, \begin{pmatrix} N_i^u \\ 0 \end{pmatrix}\right) \\ \mathcal{A}\left(\begin{pmatrix} w^* N_k^u \\ 0 \end{pmatrix}, \begin{pmatrix} 0 \\ N_i^u \end{pmatrix}\right) & \mathcal{A}\left(\begin{pmatrix} 0 \\ w^* N_k^u \end{pmatrix}, \begin{pmatrix} 0 \\ N_i^u \end{pmatrix}\right) \end{bmatrix}_{i\in I_h^u, k\in I_\Gamma},$$

$A_{33} = \mathbf{O}_{m\times m}$, and m is the degree of freedom of the pressure p,

$$\begin{bmatrix} A_{34} & A_{35} \end{bmatrix} = \left[\mathcal{B}\left(\begin{pmatrix} w^* N_k^u \\ 0 \end{pmatrix}, N_i^p\right) \ \mathcal{B}\left(\begin{pmatrix} 0 \\ w^* N_k^u \end{pmatrix}, N_i^p\right)\right]_{i\in I_h^p, k\in I_\Gamma},$$

$$\begin{bmatrix} A_{11}^{enr} & A_{12}^{enr} \\ A_{21}^{enr} & A_{22}^{enr} \end{bmatrix} = \begin{bmatrix} \mathcal{A}\left(\begin{pmatrix} w^* N_k^u \\ 0 \end{pmatrix}, \begin{pmatrix} w^* N_l^u \\ 0 \end{pmatrix}\right) & \mathcal{A}\left(\begin{pmatrix} 0 \\ w^* N_k^u \end{pmatrix}, \begin{pmatrix} w^* N_l^u \\ 0 \end{pmatrix}\right) \\ \mathcal{A}\left(\begin{pmatrix} w^* N_k^u \\ 0 \end{pmatrix}, \begin{pmatrix} 0 \\ w^* N_l^u \end{pmatrix}\right) & \mathcal{A}\left(\begin{pmatrix} 0 \\ w^* N_k^u \end{pmatrix}, \begin{pmatrix} 0 \\ w^* N_l^u \end{pmatrix}\right) \end{bmatrix}_{k,l\in I_\Gamma}$$

and $A_{21}^{enr} = (A_{12}^{enr})^T$,

$$\begin{bmatrix} F_1 \\ F_2 \end{bmatrix} = \left[\begin{pmatrix} \mathbf{f}, \begin{pmatrix} N_i^u \\ 0 \end{pmatrix} \end{pmatrix} \quad \begin{pmatrix} \mathbf{f}, \begin{pmatrix} 0 \\ N_i^u \end{pmatrix} \end{pmatrix}\right]^T_{i\in I_h^u},$$

$$\begin{bmatrix} F_1^{enr} \\ F_2^{enr} \end{bmatrix} = \left[\begin{pmatrix} \mathbf{f}, \begin{pmatrix} w^* N_l^u \\ 0 \end{pmatrix} \end{pmatrix} \quad \begin{pmatrix} \mathbf{f}, \begin{pmatrix} 0 \\ w^* N_l^u \end{pmatrix} \end{pmatrix}\right]^T_{l\in I_\Gamma}.$$

The 3×3 block matrix in the upper left corner of matrix A is the stiffness matrix for the standard FEM, namely

$$A_{3\times 3}^{fem} = \begin{bmatrix} A_{11} & A_{12} & A_{13} \\ A_{12}^T & A_{22} & A_{23} \\ A_{13}^T & A_{23}^T & A_{33} \end{bmatrix}.$$

And the subscripts 3×3 in the following matrix all refer to the corresponding block matrix. The size of the enrichment is related to the I_Γ. In addition, w^* would make the diagonal elements of the matrices A_{11}^{enr} and A_{22}^{enr} very small, so we will modify the linear system next.

3.2. The scaled condition number (SCN)

Let $H = DAD$, where D is the diagonal matrix with $D_{ii} = A_{ii}^{-1/2}$. Because of the $-1/2$, the diagonal elements of the stiffness matrix A must be greater than 0. So the zero matrix A_{33} is modified with the addition of a penalty [29,30]. The weak form (2.1) is changed to $\forall \varepsilon > 0$, find $(\mathbf{u}_\varepsilon, p_\varepsilon) \in (\mathbb{S}^k_{SGFEM} \times \mathbb{Q}_h^{k-1})$, $k = 1, 2$, such that

$$\begin{aligned} \mathcal{A}(\mathbf{u}_\varepsilon, \mathbf{v}) \ + \ \mathcal{B}(\mathbf{v}, p_\varepsilon) \ &= \ (\mathbf{f}, \mathbf{v}), \\ (\varepsilon p_\varepsilon, q) \ - \ \mathcal{B}(\mathbf{u}_\varepsilon, q) \ &= \ 0. \end{aligned} \tag{3.1}$$

There exists a unique solution to this problem. In this case, $\widetilde{A}_{33} = [(\varepsilon N_j^p, N_i^p)]_{i,j\in I_h^p}$. Since the coefficient of $\mathcal{B}(\mathbf{u}_\varepsilon, q)$ becomes -1, the final stiffness matrix is

$$A = \begin{bmatrix} A_{11} & A_{12} & A_{13} & A_{14} & A_{15} \\ A_{12}^T & A_{22} & A_{23} & A_{24} & A_{25} \\ -A_{13}^T & -A_{23}^T & \widetilde{A}_{33} & -A_{34} & -A_{35} \\ A_{14}^T & A_{24}^T & A_{34}^T & A_{11}^{enr} & A_{12}^{enr} \\ A_{15}^T & A_{25}^T & A_{35}^T & A_{21}^{enr} & A_{22}^{enr} \end{bmatrix}.$$

Note that $A_{3\times 3}^{fem}$ also changes accordingly. The scaled condition numbers (SCNs) of A and $A_{3\times 3}^{fem}$ are defined by

$$\begin{aligned} \mathcal{K}(A) &= \kappa(H) = \|H\|_2 \|H^{-1}\|_2, \\ \mathcal{K}(A_{3\times 3}^{fem}) &= \kappa(H_{3\times 3}^{fem}) = \|H_{3\times 3}^{fem}\|_2 \|(H_{3\times 3}^{fem})^{-1}\|_2, \end{aligned} \tag{3.2}$$

where $\kappa(\cdot)$ is the condition number based on the $\|\cdot\|_2$ vector norm. In the next section the SGFEM is investigated through some numerical examples.

4. Numerical experiments

$\mathcal{T}_h$ is a uniform quadrilateral mesh associated with the parameter h. The elements $\{\tau_s : s \notin E_\Gamma\}$ that do not intersect with the interface use the standard quadrilateral Gauss integration rule. For the elements $\{\tau_s : s \in E_\Gamma\}$ that intersect with the interface:

(a) if the element is divided into a triangle and a polygon (quadrilateral or pentagon) by the interface, we add the centroid to the polygon and then triangulate it;

(b) if the element is divided into two triangles or two quadrilaterals, we add the centroid to each polygon and then triangulate them.

The triangular Gauss integration rule is used in the obtained triangles. In addition, for the circular interface problem, we replace it with the polygon obtained by connecting the intersection points of the interface and the element edges. We calculate the SCNs (3.2) of the stiffness matrix for each example and the relative error as follows:

$$\|e_{\mathbf{u}}\|_{L^2} := \frac{\|\mathbf{u} - \mathbf{u}_\varepsilon\|_{L^2(\Omega)}}{\|\mathbf{u}\|_{L^2(\Omega)}}, \quad \|e_{\mathbf{u}}\|_{\mathscr{E}(\Omega)} := \frac{\|\mathbf{u} - \mathbf{u}_\varepsilon\|_{\mathscr{E}(\Omega)}}{\|\mathbf{u}\|_{\mathscr{E}(\Omega)}},$$

$$\|e_p\|_{L^2} := \frac{\|p - p_\varepsilon\|_{L^2(\Omega)}}{\|p\|_{L^2(\Omega)}}.$$

4.1. An circular interface problem

Consider the region $\Omega = (-1, 1)\times(-1, 1)$ with a uniform quadrilateral mesh. The interface is $\Gamma = \{\mathbf{x} = (x, y)^T \in \mathbb{R}^2 : x^2 + y^2 = r_0^2\}$ with $r_0 = 0.5$ and $\Omega_1 = \{(x, y) \in \Omega : x^2 + y^2 < r_0^2\}$, $\Omega_2 = \{(x, y) \in \Omega : x^2 + y^2 > r_0^2\}$. The solution $\mathbf{u}(\mathbf{x})$ and $p(\mathbf{x})$ of (3.1) are

$$\mathbf{u}(\mathbf{x}) = \begin{cases} \frac{r_0^2 - |\mathbf{x}|^2}{\mu_1}\begin{pmatrix} -y \\ x \end{pmatrix}, & \text{if } \mathbf{x} \in \Omega_1, \\ \frac{r_0^2 - |\mathbf{x}|^2}{\mu_2}\begin{pmatrix} -y \\ x \end{pmatrix}, & \text{if } \mathbf{x} \in \Omega_2, \end{cases} \quad \text{and } p(\mathbf{x}) = y^2 - x^2, \quad \mathbf{x} \in \Omega.$$

The right-hand side term $\mathbf{f}$ and the Dirichlet boundary condition $\mathbf{g}_D$ are determined by (1.1)–(1.2). In this example, for $(\mathbf{u}_\varepsilon, p_\varepsilon) \in (\mathbb{S}^1_{SGFEM} \times \mathbb{Q}_h^0)$, namely using $Q_1 - Q_0$ element for the discretization of the space $(\mathbb{S}^1_{FEM} \times \mathbb{Q}_h^0)$ and the linear interpolation function in w^*, we compute the viscosity coefficients for small and large jumps [18]: $\mu_1 = 1, \mu_2 = 5$; $\mu_1 = 5, \mu_2 = 1$; $\mu_1 = 1000, \mu_2 = 1$ and $\varepsilon = 10^{-6}$ in (3.1). The errors and their convergence orders are shown in Tables 1–3.

From the results, both the relative L^2 error and the relative energy error for velocity $\mathbf{u}$ at the same optimal convergence orders as Remark 1, which are $O(h^2)$ and $O(h)$, respectively. And the order of convergence of the relative L^2 error for pressure p is $O(h)$. The absolute errors are only slightly larger than the relative errors. Compared with [18], most of the errors are smaller.

The study of SCNs for A and $A_{3\times 3}^{fem}$ as shown in Fig. 4. It shows the comparison between $\mathcal{K}(A)$ and $\mathcal{K}(A_{3\times 3}^{fem})$ under three different viscosity ratio values. As the grid is refined, the growth rate of $\mathcal{K}(A)$ remains at $O(h^{-2})$, which is the same as $\mathcal{K}(A_{3\times 3}^{fem})$ in the standard FEM. Although A has more degrees of freedom than $A_{3\times 3}^{fem}$, their SCNs are very similar. These results indicate that SGFEM has a well-conditioned stiffness matrix and avoids pathological problems.

4.2. An straight interface problem

Consider the example 4.1 from [19]. The region is $\Omega = (-1, 1)\times(-1, 1)$ with a straight interface $\Gamma = \{\mathbf{x} = (x, y)^T \in \mathbb{R}^2 : 2x + y - c = 0\}$, where $c = \sqrt{2}$. And $\Omega_1 = \{(x, y) \in \Omega : 2x + y - c > 0\}, \Omega_2 = \{(x, y) \in \Omega : 2x + y - c < 0\}$. The solution $\mathbf{u}(\mathbf{x})$ and $p(\mathbf{x})$ are

$$\mathbf{u} = \begin{cases} \begin{pmatrix} (2x + y - c)^3/(2\mu_1) \\ -(2x + y - c)^3/\mu_1 \end{pmatrix}, & (x, y) \in \Omega_1, \\ \begin{pmatrix} (2x + y - c)^3/(2\mu_2) \\ -(2x + y - c)^3/\mu_2 \end{pmatrix}, & (x, y) \in \Omega_2, \end{cases} \quad \text{and} \quad p = e^x - e^y.$$

The discretization of the space $(\mathbb{S}^2_{FEM} \times \mathbb{Q}_h^1)$ uses the Taylor-Hood element for $(\mathbf{u}_\varepsilon, p_\varepsilon) \in (\mathbb{S}^2_{SGFEM} \times \mathbb{Q}_h^1)$. Note here that the interpolation function in w^* is quadratic. We test the convergence performance for both small and large jumps, namely $\mu_1 = 1, \mu_2 = 10$; $\mu_1 = 10, \mu_2 =$

Table 1
Relative error of the SGFEM with $\mu_1 = 1, \mu_2 = 5, \varepsilon = 10^{-6}$.

h^{-1}	$\|e_{\mathbf{u}}\|_{L^2}$	Order	$\|e_{\mathbf{u}}\|_{\mathscr{E}(\Omega)}$	Order	$\|e_p\|_{L^2}$	Order
8	1.5175×10^{-2}	–	8.6560×10^{-2}	–	1.4178×10^{-1}	–
16	3.8048×10^{-3}	1.9958	4.4828×10^{-2}	0.9493	7.4429×10^{-2}	0.9298
32	1.0229×10^{-3}	1.8951	2.2463×10^{-2}	0.9968	3.9645×10^{-2}	0.9087
64	2.5690×10^{-4}	1.9934	1.1728×10^{-2}	0.9376	1.9172×10^{-2}	1.0482
128	6.5399×10^{-5}	1.9739	5.7943×10^{-3}	1.0173	9.9365×10^{-3}	0.9482
256	1.7597×10^{-5}	1.8939	3.0108×10^{-3}	0.9445	5.0008×10^{-3}	0.9906

Table 2
Relative error of the SGFEM with $\mu_1 = 5, \mu_2 = 1, \varepsilon = 10^{-6}$.

h^{-1}	$\|e_{\mathbf{u}}\|_{L^2}$	Order	$\|e_{\mathbf{u}}\|_{\mathscr{E}(\Omega)}$	Order	$\|e_p\|_{L^2}$	Order
8	1.3707×10^{-2}	–	8.1777×10^{-2}	–	1.4167×10^{-1}	–
16	3.4363×10^{-3}	1.9960	4.1015×10^{-2}	0.9956	7.3364×10^{-2}	0.9495
32	8.6069×10^{-4}	1.9973	2.0520×10^{-2}	0.9991	3.6064×10^{-2}	1.0245
64	2.1534×10^{-4}	1.9989	1.0292×10^{-2}	0.9956	1.8121×10^{-2}	0.9929
128	5.3845×10^{-5}	1.9997	5.1441×10^{-3}	1.0005	9.1008×10^{-3}	0.9936
256	1.3465×10^{-5}	1.9996	2.5772×10^{-3}	0.9971	4.6435×10^{-3}	0.9708

Table 3
Relative error of the SGFEM with $\mu_1 = 1000, \mu_2 = 1, \varepsilon = 10^{-6}$.

h^{-1}	$\|e_{\mathbf{u}}\|_{L^2}$	Order	$\|e_{\mathbf{u}}\|_{\mathscr{E}(\Omega)}$	Order	$\|e_p\|_{L^2}$	Order
8	2.1477×10^{-2}	–	4.6880×10^{-1}	–	6.6372×10^{-1}	–
16	5.2980×10^{-3}	2.0193	1.3394×10^{-1}	1.8074	5.9079×10^{-1}	0.1679
32	1.0560×10^{-3}	2.3269	2.8968×10^{-2}	2.2091	1.7653×10^{-1}	1.7427
64	2.2956×10^{-4}	2.2016	1.0879×10^{-2}	1.4129	7.5925×10^{-2}	1.2173
128	5.4775×10^{-5}	2.0673	5.2056×10^{-3}	1.0634	2.7969×10^{-2}	1.4407
256	1.3571×10^{-5}	2.0130	2.5767×10^{-3}	1.0146	1.6699×10^{-2}	0.7441

Table 4
Relative error of the SGFEM with $\mu_1 = 1, \mu_2 = 10, \varepsilon = 10^{-8}$.

h^{-1}	$\|e_{\mathbf{u}}\|_{L^2}$	Order	$\|e_{\mathbf{u}}\|_{\mathscr{E}(\Omega)}$	Order	$\|e_p\|_{L^2}$	Order
4	8.1943×10^{-4}	–	4.6850×10^{-3}	–	3.2223×10^{-2}	–
8	1.0114×10^{-4}	3.0183	1.1617×10^{-3}	2.0119	6.8160×10^{-3}	2.2411
16	1.2711×10^{-5}	2.9923	2.9298×10^{-4}	1.9873	8.1907×10^{-4}	3.0569
32	1.5857×10^{-6}	3.0028	7.3195×10^{-5}	2.0010	1.5076×10^{-4}	2.4417
64	1.9930×10^{-7}	2.9921	1.8389×10^{-5}	1.9929	2.5699×10^{-5}	2.5525
128	2.5082×10^{-8}	2.9902	4.5952×10^{-6}	2.0006	5.6675×10^{-6}	2.1809

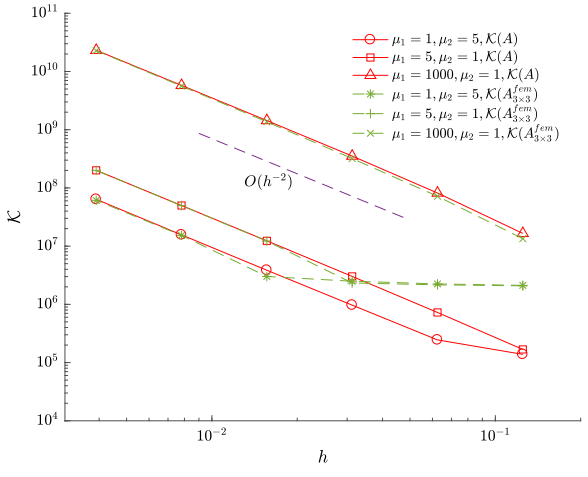

Fig. 4. Comparison of $\mathcal{K}(A)$ and $\mathcal{K}(A^{fem}_{3\times3})$ under different μ_1 and μ_2 in the circular interface example.

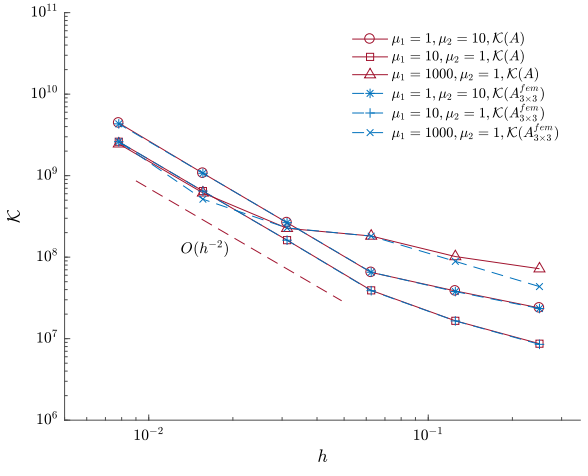

Fig. 5. Comparison of $\mathcal{K}(A)$ and $\mathcal{K}(A^{fem}_{3\times3})$ under different μ_1 and μ_2 in the straight interface example.

1; $\mu_1 = 1000, \mu_2 = 1$ and $\varepsilon = 10^{-8}$ in (3.1). The errors and their convergence orders are shown in Tables 4–6.

Similarly, the relative L^2 error and relative energy error for velocity $\mathbf{u}$ also achieve the same optimal convergence orders as Remark 1, which

Table 5
Relative error of the SGFEM with $\mu_1 = 10, \mu_2 = 1, \varepsilon = 10^{-8}$.

h^{-1}	$\|e_{\mathbf{u}}\|_{L^2}$	Order	$\|e_{\mathbf{u}}\|_{\mathcal{E}(\Omega)}$	Order	$\|e_p\|_{L^2}$	Order
4	1.8643×10^{-4}	–	2.8203×10^{-3}	–	1.7016×10^{-2}	–
8	2.3294×10^{-5}	3.0006	7.0721×10^{-4}	1.9956	2.8801×10^{-3}	2.5627
16	2.9177×10^{-6}	2.9971	1.7714×10^{-4}	1.9973	5.5722×10^{-4}	2.3698
32	3.6490×10^{-7}	2.9992	4.4337×10^{-5}	1.9983	1.0505×10^{-4}	2.4071
64	4.5655×10^{-8}	2.9987	1.1094×10^{-5}	1.9988	2.4392×10^{-5}	2.1066
128	5.7168×10^{-9}	2.9975	2.7738×10^{-6}	1.9998	5.3152×10^{-6}	2.1982

Table 6
Relative error of the SGFEM with $\mu_1 = 1000, \mu_2 = 1, \varepsilon = 10^{-8}$.

h^{-1}	$\|e_{\mathbf{u}}\|_{L^2}$	Order	$\|e_{\mathbf{u}}\|_{\mathcal{E}(\Omega)}$	Order	$\|e_p\|_{L^2}$	Order
4	2.4034×10^{-4}	–	3.7808×10^{-3}	–	5.1234×10^{-1}	–
8	2.6446×10^{-5}	3.1839	7.7361×10^{-4}	2.2890	6.1362×10^{-2}	3.0617
16	3.1628×10^{-6}	3.0638	1.8261×10^{-4}	2.0828	1.1476×10^{-2}	2.4188
32	3.7480×10^{-7}	3.0770	4.4644×10^{-5}	2.0322	1.0579×10^{-3}	3.4394
64	4.6634×10^{-8}	3.0067	1.1102×10^{-5}	2.0076	2.4378×10^{-4}	2.1175
128	5.7345×10^{-9}	3.0236	2.7544×10^{-6}	2.0110	4.3495×10^{-5}	2.4867

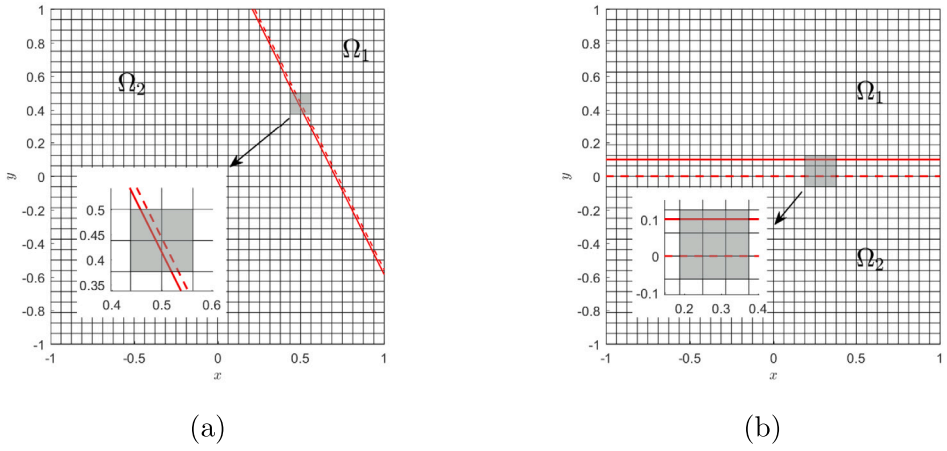

Fig. 6. The change of the interface with δ: (a) Γ_1 with δ_1. (b) Γ_2 with δ_2.

are $O(h^3)$ and $O(h^2)$, respectively. And the order of convergence of the relative L^2 error for pressure p is $O(h^2)$. The study on SCNs are shown in Fig. 5. It also demonstrates the comparison between $\mathcal{K}(A)$ and $\mathcal{K}(A^{fem}_{3\times3})$ under three different viscosity ratio values. We can draw the same conclusion as the circular example: the growth rate of $\mathcal{K}(A)$ is the same as that of $\mathcal{K}(A^{fem}_{3\times3})$, both being $O(h^{-2})$. And the SCNs of A and $A^{fem}_{3\times3}$ are similar.

4.3. The SCNs of stiffness matrix and robustness

In this section, the scaled condition number of the stiffness matrix and the robustness of the SGFEM are investigated by using the straight interface. The interface too close to the mesh nodes or edges often occurs in moving interface problems. Therefore, here we artificially make the straight interface closer to the mesh nodes by adding a parameter δ_1 or δ_2. Consider the interface of Section 4.2

$$\Gamma_1 = \{\mathbf{x} = (x, y)^T \in \mathbb{R}^2 : 2x + y - c - \delta_1 = 0\}.$$

Consider another interface parallel to the mesh edges

$$\Gamma_2 = \{\mathbf{x} = (x, y)^T \in \mathbb{R}^2 : y = \delta_2\}.$$

The mesh step h is fixed to $(\frac{1}{16}, \frac{1}{16})$ and we gradually change δ_1 and δ_2. The straight interface moves from solid line to dashed line so that it is close to the mesh nodes or edges, see Fig. 6. The interface Γ_1 approaches the nodes continuously and Γ_2 almost coincides with the mesh lines.

The results of SCNs are shown in Fig. 7. Obviously, as δ_1 or δ_2 changes, no matter how close the interface is to the mesh, the scaled condition number of the stiffness matrix $\mathcal{K}(A)$ is almost unchanged. It means that SGFEM avoids the problem of the surge in the condition number in traditional GFEM and has robustness in adjusting the grid. This conclusion is ideal.

In addition, the enrichment nodes were treated according to Fig. 2 during the study, but the errors were not stable. This further illustrates the convenience and stability of SGFEM.

5. Conclusion

This paper investigates the error convergence and robustness of the SGFEM when applied to the Stokes interface problems. The study of two numerical examples reveals that the error convergence order of the SGFEM is the same as that of the traditional FEM solving Stokes equations without an interface. The SCN of the stiffness matrix has the same growth order as that of the standard FEM part. Even when the interface is close to the mesh nodes or edges, the SCN of the SGFEM does not change significantly. These results demonstrate that SGFEM overcomes the interface problems and the drawbacks of the traditional GFEM. It has a well-conditioned stiffness matrix, robustness and the optimal error convergence order. This is important for further research on moving interface problems.

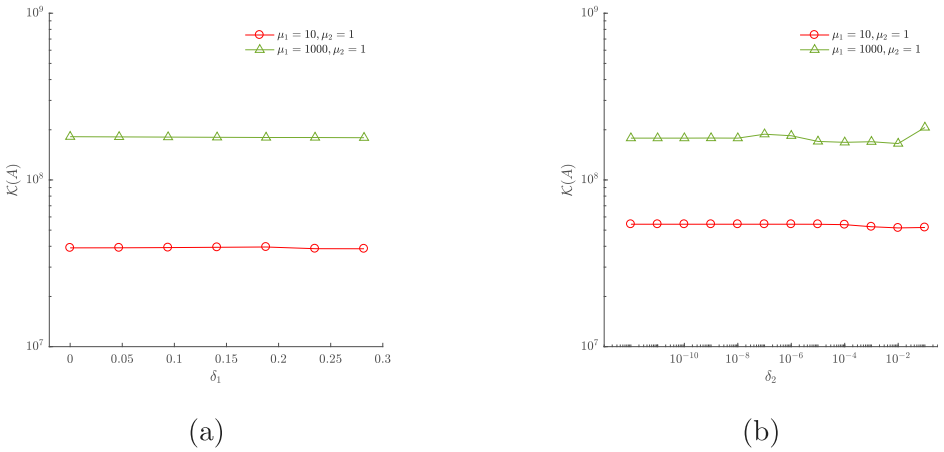

Fig. 7. Variation of $\mathcal{K}(A)$ with interface movement: (a) Γ_1 with δ_1. (b) Γ_2 with δ_2.

CRediT authorship contribution statement

Haodi Zhu: Writing – original draft, Visualization, Software, Methodology, Investigation. **Jianping Zhao:** Writing – review & editing. **Yanren Hou:** Writing – review & editing.

Declaration of competing interest

The authors declare no potential conflict of interests. The authors declare that they have no known competing financial interests or personal relationships that could have appeared to influence the work reported in this paper.

Data availability

No data was used for the research described in the article.

Acknowledgments

This work was partially supported by grants from the Xinjiang Uygur Autonomous Region Natural Science Fund (No. 2022D01C409), National Key R&D Program of China (No. 2022YFA1004402) and the National Natural Science Foundation of China (No. 61962056). We are grateful to the reviewers and editors.

References

[1] Peskin CS. Flow patterns around heart valves: A numerical method. J Comput Phys 1972;10(2):252–71.
[2] LeVeque RJ, Li Z. The immersed interface method for elliptic equations with discontinuous coefficients and singular sources. SIAM J Numer Anal 1994;31(4):1019–44.
[3] Zhao J, Hou Y, Li Y. Immersed interface method for elliptic equations based on piecewise second order polynomial. Comput Math Appl 2012;63(5):957–65.
[4] Babuška I, Caloz G, Osborn Osborn JE. Special finite element methods for a class of second order elliptic problems with rough coefficients. SIAM J Numer Anal 1994;31(4):945–81.
[5] Melenk JM, Babuška I. The partition of unity finite element method: Basic theory and applications. Comput Methods Appl Mech Engrg 1996;139(1–4):289–314.
[6] Dolbow JE. An extended finite element method with discontinuous enrichment for applied mechanics [Ph. D. thesis], Northwesten University; 1999, Theoretical and Applied Mechanics.
[7] Moës N, Dolbow J, Belytschko T. A finite element method for crack growth without remeshing. Internat J Numer Methods Engrg 1999;46(1):131–50.
[8] Sukumar N, Prevost JH. Modeling quasi-static crack growth with the extended finite element method part I: Computer implementation. Int J Solids Struct 2003;40(26):7513–37.
[9] Daux C, Moës N, Dolbow J, et al. Arbitrary branched and intersecting cracks with the extended finite element method. Internat J Numer Methods Engrg 2000;48(12):1741–60.
[10] Strouboulis T, Babuška I, Copps K. The design and analysis of the generalized finite element method. Comput Methods Appl Mech Engrg 2000;181(1–3):43–69.
[11] Strouboulis T, Copps K, Babuška I. The generalized finite element method: An example of its implementation and illustration of its performance. Internat J Numer Methods Engrg 2000;47(8):1401–17.
[12] Strouboulis T, Copps K, Babuška I. The generalized finite element method. Comput Methods Appl Mech Engrg 2001;190(32–33):4081–193.
[13] Fries TP, Belytschko T. The extended/generalized finite element method: An overview of the method and its applications. Internat J Numer Methods Engrg 2010;84(3):253–304.
[14] Hansbo A, Hansbo P. An unfitted finite element method, based on Nitsche's method, for elliptic interface problems. Comput Methods Appl Mech Eng 2002;191(47–48):5537–52.
[15] Cattaneo L, Formaggia L, Iori GF, et al. Stabilized extended finite elements for the approximation of saddle point problems with unfitted interface. Calcolo 2015;52(2):123–52.
[16] Capatina D, El-Otmany H, Graebling D, et al. Extension of NXFEM to nonconforming finite elements. Math Comput Simulation 2017;137:226–45.
[17] Guzmán J, Olshanskii M. Inf-sup stability of geometrically unfitted Stokes finite elements. Math Comp 2018;87(313):2091–112.
[18] Ji H, Wang F, Chen J, et al. An immersed CR-P0 element for Stokes interface problems and the optimal convergence analysis. Comput Methods Appl Mech Engrg 2022;399:115306.
[19] Chen Y, Zhang X. A P2-P1 partially penalized immersed finite element method for Stokes interface problems. Int J Num Anal Model 2021;18(1):120–41.
[20] Wang N, Chen J. A nonconforming nitsches extended finite element method for Stokes interface problems. J Sci Comput 2019;81:342–74.
[21] Babuška I, Banerjee U. Stable generalized finite element method (SGFEM). Comput Methods Appl Mech Engrg 2012;201:91–111.
[22] Kergrene K, Babuška I, Banerjee U. Stable generalized finite element method and associated iterative schemes; Application to interface problems. Comput Methods Appl Mech Engrg 2016;305:1–36.
[23] Sauerl H, Fries TP. The stable XFEM for two phase flows. Comput & Fluids 2013;87:41–9.
[24] Gupta V, Duarte CA, Babuška I, et al. Stable GFEM (SGFEM): Improved conditioning and accuracy of GFEM/XFEM for three-dimensional fracture mechanics. Comput Methods Appl Mech Engrg 2015;289:355–86.
[25] Zhang Q, Babuška I. A stable generalized finite element method (SGFEM) of degree two for interface problems. Comput Methods Appl Mech Eng 2020;363:112889.
[26] Zhang Q, Banerjee U, Babuška I. Higher order stable generalized finite element method. Numer Math 2014;128(1):1–29.
[27] Zhu P, Zhang Q. BDF schemes in stable generalized finite element methods for parabolic interface problems with moving interfaces. CMES-Comput Model Eng Sci 2020;124(1):107–27.
[28] Zhu P, Zhang Q, Liu T. Stable generalized finite element method (SGFEM) for parabolic interface problems. J Comput Appl Math 2020;367:112475.
[29] Girault V, Raviart PA. Finite element methods for Navier–Stokes equations: theory and algorithms. Springer Science & Business Media; 2012.
[30] Li K, Ma Y. Hilbert space methods for mathematical physics equations(in Chinese). Science Press; 2008.